Cell Reports
Medicine

Article

Genetic resiliency associated with dominant lethal *TPM1* mutation causing atrial septal defect with high heritability

Graphical abstract

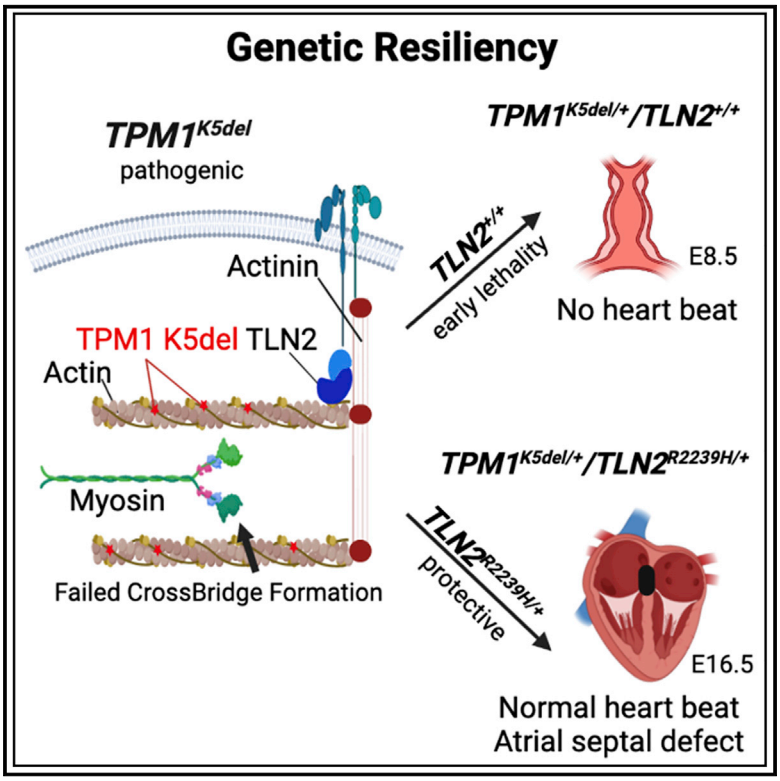

Highlights

- *TPM1* mutation linked to atrial septal defect causes embryonic death with no heartbeat
- *TLN2* identified as protective variant suppressing the deleterious *TPM1* mutation
- CRISPR *Tpm1*/*Tln2* double-KI mice show rescued heart beating and atrial septal defects
- Functional annotation of variants of unknown significance with CRISPR founder analysis

Authors

Polakit Teekakirikul, Wenjuan Zhu, Xinxiu Xu, ..., Hui Zhao, Brian Feingold, Cecilia W. Lo

Correspondence

cel36@pitt.edu

In brief

Pathogenic mutations known to cause severe disease can be found in healthy individuals, but the mechanism remains unknown. Teekakirikul et al. show suppression of embryonic lethality of a rare *TPM1* mutation by suppressor variant in *TLN2*. Rescue of embryonic lethality also uncovers a role for *TPM1* in atrial septal defect.

Teekakirikul et al., 2022, Cell Reports Medicine *3*, 100501
February 15, 2022
https://doi.org/10.1016/j.xcrm.2021.100501

CellPress

Cell Reports Medicine

CellPress
OPEN ACCESS

Article

Genetic resiliency associated with dominant lethal *TPM1* mutation causing atrial septal defect with high heritability

Polakit Teekakirikul,[1,2,3,19] Wenjuan Zhu,[3,4,19] Xinxiu Xu,[1,19] Cullen B. Young,[1,19] Tuantuan Tan,[1] Amanda M. Smith,[5] Chengdong Wang,[6] Kevin A. Peterson,[7] George C. Gabriel,[1] Sebastian Ho,[1] Yi Sheng,[8] Anne Moreau de Bellaing,[1] Daniel A. Sonnenberg,[1] Jiuann-huey Lin,[9] Elisavet Fotiou,[10] Gennadiy Tenin,[10] Michael X. Wang,[1] Yijen L. Wu,[1] Timothy Feinstein,[1] William Devine,[1] Honglan Gou,[11] Abha S. Bais,[1] Benjamin J. Glennon,[1] Maliha Zahid,[1] Timothy C. Wong,[12] Ferhaan Ahmad,[13] Michael J. Rynkiewicz,[14] William J. Lehman,[14] Bernard Keavney,[10] Tero-Pekka Alastalo,[15] Mary-Louise Freckmann,[16] Kyle Orwig,[8] Steve Murray,[7] Stephanie M. Ware,[5] Hui Zhao,[6,17] Brian Feingold,[18] and Cecilia W. Lo[1,20,*]

[1]Department of Developmental Biology, University of Pittsburgh School of Medicine, Pittsburgh, PA, USA
[2]Division of Cardiology, Department of Medicine & Therapeutics, The Chinese University of Hong Kong, Hong Kong SAR, China
[3]Centre for Cardiovascular Genomics & Medicine, The Chinese University of Hong Kong, Hong Kong SAR, China
[4]Division of Medical Sciences, Department of Medicine & Therapeutics, The Chinese University of Hong Kong, Hong Kong SAR, China
[5]Department of Pediatrics and Department of Medical and Molecular Genetics, and Herman B Wells Center for Pediatric Research, Indiana University School of Medicine, Indianapolis, IN, USA
[6]School of Biomedical Sciences, The Chinese University of Hong Kong, Hong Kong SAR, China
[7]The Jackson Laboratory, Bar Harbor, ME, USA
[8]Magee-Womens Research Institute, University of Pittsburgh School of Medicine, Pittsburgh, PA, USA
[9]Department of Critical Care Medicine, University of Pittsburgh School of Medicine, Pittsburgh, PA, USA
[10]Division of Cardiovascular Sciences, Faculty of Biology, Medicine and Health, University of Manchester, Manchester, UK
[11]BGI Genomics, Shenzhen, China
[12]UPMC Heart and Vascular Institute and Division of Cardiology, University of Pittsburgh School of Medicine, Pittsburgh, PA, USA
[13]Division of Cardiovascular Medicine, Department of Internal Medicine, The University of Iowa, Iowa City, IA, USA
[14]Department of Physiology & Biophysics, Boston University School of Medicine, Boston, MA, USA
[15]Blueprint Genetics, San Francisco, CA, USA
[16]Department of Clinical Genetics, Royal North Shore Hospital, Sydney, NSW, Australia
[17]Hong Kong Branch of CAS Center for Excellence in Animal Evolution and Genetics, The Chinese University of Hong Kong, Hong Kong SAR, China
[18]Heart Institute and Division of Pediatric Cardiology, Children's Hospital of Pittsburgh of UPMC, Pittsburgh, PA, USA
[19]These authors contributed equally
[20]Lead contact
*Correspondence: cel36@pitt.edu
https://doi.org/10.1016/j.xcrm.2021.100501

SUMMARY

Analysis of large-scale human genomic data has yielded unexplained mutations known to cause severe disease in healthy individuals. Here, we report the unexpected recovery of a rare dominant lethal mutation in *TPM1*, a sarcomeric actin-binding protein, in eight individuals with large atrial septal defect (ASD) in a five-generation pedigree. Mice with *Tpm1* mutation exhibit early embryonic lethality with disrupted myofibril assembly and no heartbeat. However, patient-induced pluripotent-stem-cell-derived cardiomyocytes show normal beating with mild myofilament defect, indicating disease suppression. A variant in *TLN2*, another myofilament actin-binding protein, is identified as a candidate suppressor. Mouse CRISPR knock-in (KI) of both the *TLN2* and *TPM1* variants rescues heart beating, with near-term fetuses exhibiting large ASD. Thus, the role of *TPM1* in ASD pathogenesis unfolds with suppression of its embryonic lethality by protective *TLN2* variant. These findings provide evidence that genetic resiliency can arise with genetic suppression of a deleterious mutation.

INTRODUCTION

Recent large-scale acquisition of human next-generation sequencing data has led to rapid progress in the identification of monogenic causes of Mendelian diseases.[1] This has yielded increasing evidence for the incomplete penetrance of many heritable diseases, with some striking examples noted in a study reporting 13 individuals with pathogenic mutations known to cause severe Mendelian diseases, but without evidence of disease.[2] Such genetic resiliency is suggested to

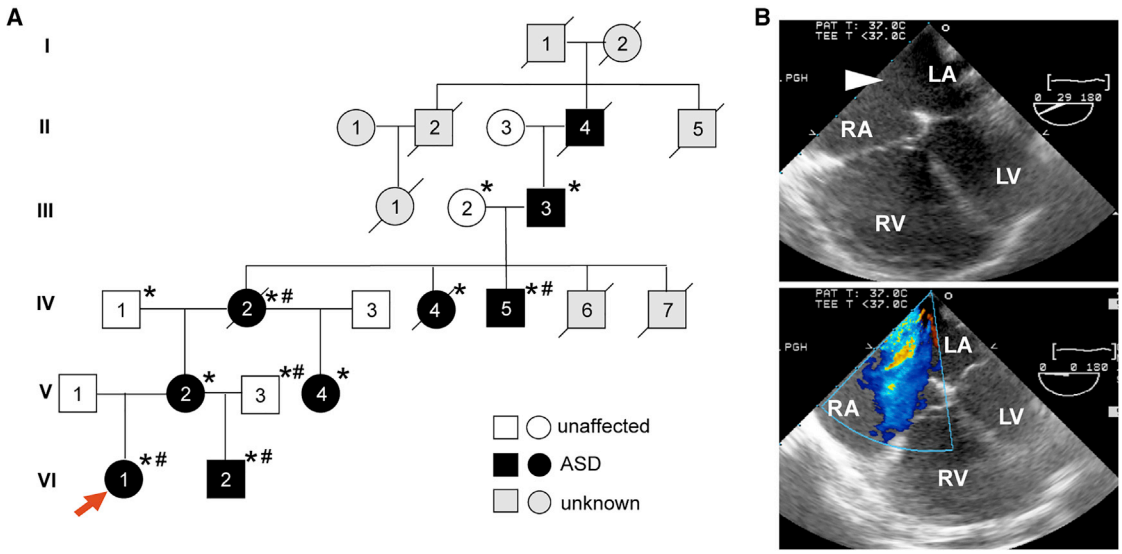

Figure 1. Pedigree and echocardiograph of familial ASD

(A) A five-generation pedigree with ASDs was recruited with the proband indicated by arrow. Deceased subjects are indicated with diagonal line, with subjects II-5, III-1, IV-6, and IV-7 being miscarriages. Subjects included in the linkage analysis (asterisk) and WGS (pound sign) are as indicated. Square, male subject; circle, female subject.

(B) Transesophageal echocardiography of index patient shows large secundum ASD (upper white arrow) with color Doppler showing blood shunting from left (LA) to right atrium (RA).

reflect the suppression of pathogenic mutations by protective variants in other genes. While this concept is appealing, no study has yet provided experimental evidence documenting such genetic buffering by protective variants. In the present study, we obtained evidence for such disease suppression in studies investigating the genetic etiology of atrial septal defect (ASD), a congenital heart disease (CHD) comprising a hole in the heart.

CHD is one of the most common birth defects, affecting 1% of live births.[3–6] A genetic etiology is indicated by the increased recurrence risk among family members and also the association of CHD with chromosomal anomalies in syndromic disorders.[7,8] In ASDs, a hole in the atrial septum allows shunting of blood from the left (LA) to the right atrium (RA) and is one of the most common CHDs. Most ASDs involve a defect in the septum secundum derived from infolding of the roof of the atria. Secundum ASD was one of the first CHDs shown to have high recurrence risk[9–11] and also the first CHD for which a disease-causing gene was identified, *NKX2.5*.[12] Several other transcription factors and also sarcomeric genes (*ACTC1*, *MYH6*) have been identified or implicated to cause ASDs.[10,13–17] However, the genetic etiology for the vast majority of ASDs remain unexplained, with both recessive and dominant inheritance patterns of transmission reported.[18] Studies conducted in inbred mice showed the presence of genetic modifiers for ASD and other CHDs.[19,20] Interestingly, this was shown to mostly buffer the CHD-causing mutation against disease.[19] Quantitative trait loci (QTL) mapping in mice also successfully identified multiple independent loci for patent foramen ovale,[21] a phenotype closely related to ASD. However, recovery of the genes contributing to genetic buffering or underlying the QTL is still challenging.

In the present study, we document a multigenerational, nonconsanguineous Caucasian pedigree exhibiting secundum ASD transmitted with complete penetrance. Using genomic approaches and animal modeling, we showed the highly heritable ASD phenotype has a digenic etiology involving an embryonic lethal pathogenic variant in *TPM1* and a protective variant in *TLN2*, two proteins with important roles in sarcomeric actin assembly.

RESULTS

We recruited a family of 11 individuals spanning five generations in which 8 family members have large ASDs (Figure 1A). While small ASDs can close spontaneously, the large secundum ASDs in this family required surgical patch repair at birth (Figure 1B). The brother (VI-2) of the index patient also exhibited transient dilated cardiomyopathy (DCM) that resolved. Two of the affected family members, IV-2 and IV-4, suffered sudden death in mid- to late adult life (Figure 1A). The ASD phenotype showed complete penetrance in every generation. Notable is the union of one parent with two different unaffected partners in generations IV and V, yielding two offspring with ASD in generations V and VI, respectively (Figure 1). Together with the overall pattern of inheritance observed over the five generations, this would suggest a dominant genetic model of disease.

Linkage analysis and WGS identifies rare *TPM1* pathogenic variant

To investigate the genetic etiology of the ASDs in this multigenerational family, we conducted genome-wide linkage analysis on the proband, as well as seven affected and three unaffected family members (denoted by asterisks in Figures 1A and S1). This

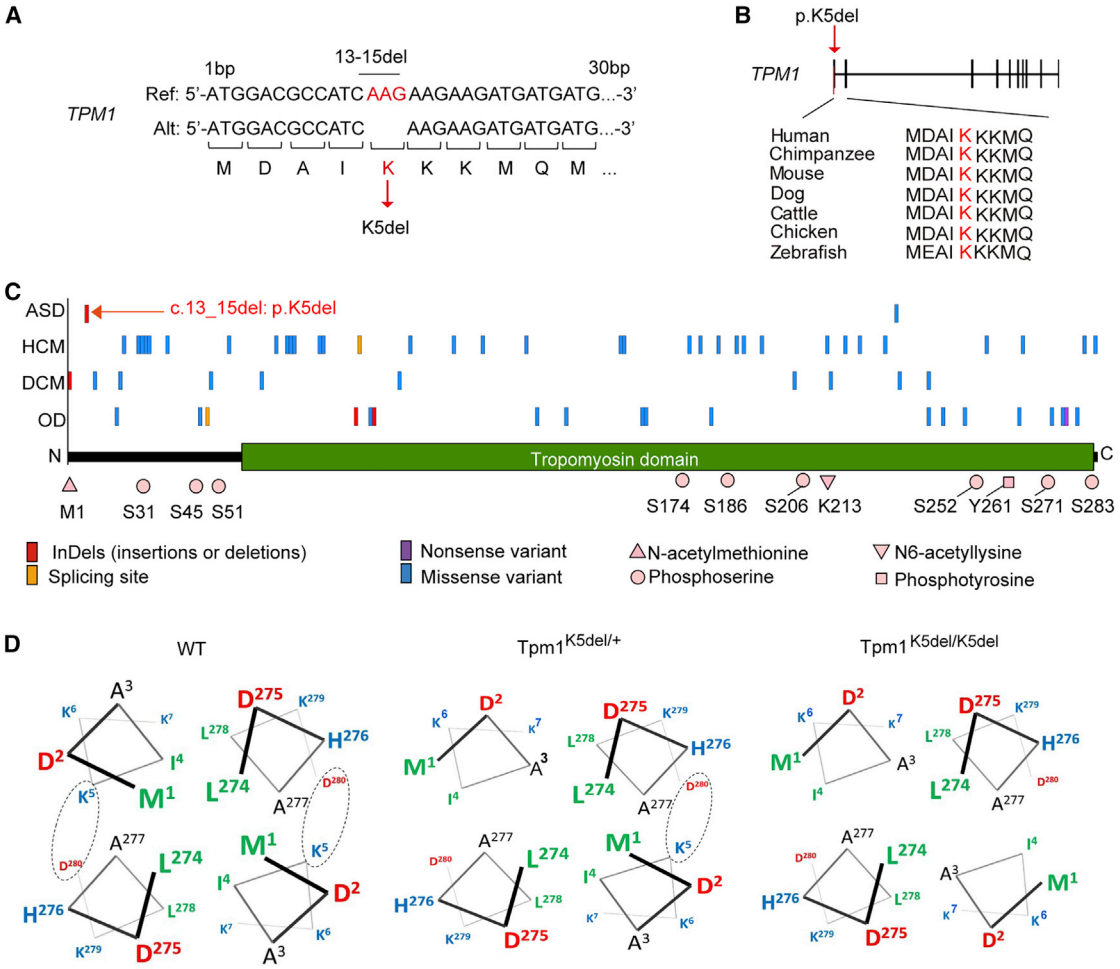

Figure 2. *TPM1* variants and impact of K5del mutation on protein structure

(A) Position of the c.13_15del variant (rs730881155) recovered and the resulting loss of one of three consecutive lysine residues at the 5′ end of the TPM1 protein is shown.

(B) *TPM1*^{K5del} mutation deletes one of three highly conserved consecutive lysine residues at the N terminus of TPM1.

(C) Position of *TPM1* variants associated with ASD (this study), dilated cardiomyopathy (DCM), and hypertrophic cardiomyopathy (HCM). ODs, other cardiac defects.

(D) Helical wheel diagrams of rat α-tropomyosin using the published model of the tropomyosin cable (19). Residues are shown in approximate location in space, with smaller text oriented away from the viewer. Residues are colored by type, with positive (blue), negative (red), and hydrophobic (green) residues highlighted. Middle (*Tpm1*$^{K5del/+}$) and right (*Tpm1*$^{K5del/K5del}$) show Lys5 deletion effectively shifts all N-terminal residues one helical position away from viewer in the context of either heterodimers comprising heterozygous and WT TPM1 (middle panel) or homodimers comprising only the mutant TPM1 protein (right panel).

analysis yielded three regions, with the maximum peak log-of-odds (LOD) score (LOD = 1.806, not significant due to limited sample size) at chromosomal intervals 8p11.23-q11.23, 15q22.2-q26.1, and 18q21.2 (Data S1; Figure S1B). Three haplotypes were constructed over these three linkage intervals, none of which were detected in the general population. All three linkage regions segregated with ASDs in this family. Only the 18q21.2 interval was previously reported to be associated with diverse CHDs.[22]

To recover candidate genes in the linkage intervals, whole genome sequencing (WGS) analysis was conducted for the proband, three affected, and one unaffected family member from generations III, IV, and V (Figure 1A; Data S1). Filtering for rare variants with minor allele frequency (MAF) < 0.01 with predicted protein coding changes yielded seven variants shared by all four affected individuals, but not by the unaffected family member (Data S1). Of these, only one variant was found within one of the three chromosome intervals identified in the linkage analysis: a heterozygous 3-base in-frame deletion variant (c.13_15del; p.K5del) causing loss of a highly conserved N-terminal lysine (Human Genome Variation Society annotation of variant as c.20_22del; p.K7del) in *TPM1* encoding α-tropomyosin (Figures 2A and 2B).

Extreme rarity of the *TPM1* mutation

α-tropomyosin is a highly conserved sarcomeric actin-binding protein expressed in the heart, skeletal, and smooth muscles

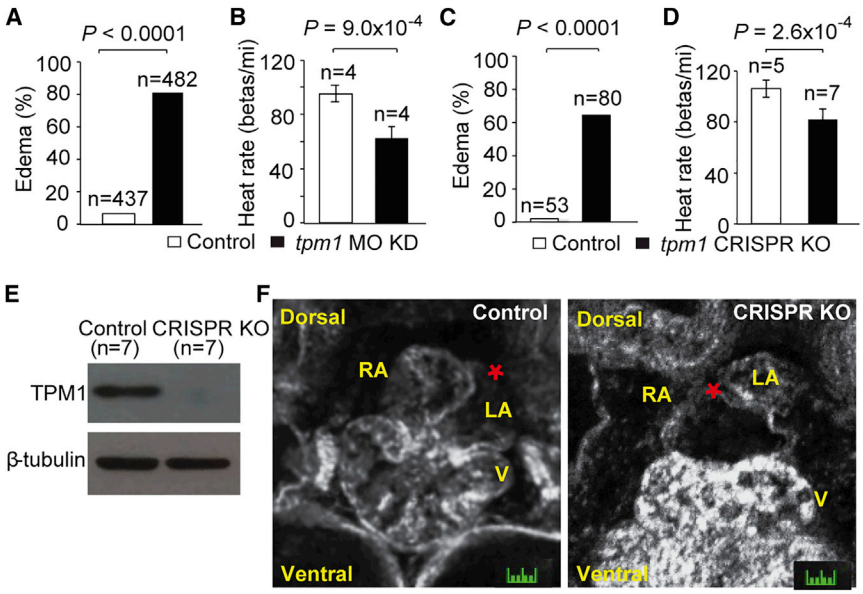

Figure 3. Functional assessments of *tpm1* deficiency on heart development in *Xenopus* embryos

(A and B) Quantification of edema/pericardial effusion (A) and heart rate (B) in *tpm1* MO KD in *Xenopus laevis* embryos.

(C and D) Quantification of edema/pericardial effusion (C) and heart rate (D) in *tpm1* CRISPR-Cas9 KO in *Xenopus tropicalis* embryos.

(E) Western blot showed TPM1 protein expression is extinguished in CRISPR-Cas9 *tpm1* KO *Xenopus tropicalis* embryos (n = number of embryos analyzed)

(F) Representative histological section of stage 40 *Xenopus tropicalis* embryo with *tpm1* CRISPR KO showed ASD (red asterisk), compared to control embryo with atrial septum (red asterisk). Scale bar, 10 μm.

In (A)–(E), n = number of *Xenopus* embryos examined. Data for (A)–(E) are represented as mean ± SEM and analyzed using unpaired Student's t test.

and in the cytoskeleton of non-muscle cells.[23] Sanger sequencing confirmed this *TPM1* mutation is present in all affected, but not in any unaffected, family members (Figure S1). This mutation was found in heterozygosity throughout the pedigree, supporting a dominant model of disease. It was not observed in any public databases (Figure 2C; Data S1) and is reported in only three other individuals worldwide as a variant of unknown significance (VUS) in ClinVar (VCV000181682.4; see Data S1). This mutation was not detected in further screening of >900 unrelated simple and complex CHD cases (all white), 111 of whom have isolated ASDs and 94 inherited cardiomyopathy cases.

TPM1 mutation may exert dominant-negative effects

The α-tropomyosin protein forms an α-helical coiled-coiled dimer assembled in head-to-tail fashion, helping to stabilize actin filaments[24] and regulate actomyosin cross-bridge formation.[25] Modeling using a 4-helix bundle showed the N-terminal region spanning the K5del mutation is stabilized by a hydrophobic core (Met1, Ile4,Leu274,Leu278) with an interchain salt bridge between Lys5 and Asp280 (Figure 2D, left). Lys5 loss would predict rotation of the Met1 and Ile4 away from the helical bundle center and replacement with a single Ala (Ala3; Figure 2D, middle). As a result, Ile4 would occupy the position normally occupied by Lys5, causing loss of the interchain salt bridge. These structural changes either in heterozygosity ($TPM1^{K5del/+}$) or homozygosity ($TPM1^{K5del/K5del}$) (Figures 2D and 2E, middle and right) are likely to destabilize the dimeric complex and, thus, alter its interactions with troponin T. This would predict a disruption of myofilament assembly and actomyosin cross-bridge formation that could lead to loss of contractility. Consistent with this, the *Tpm1* knockout (KO) mice have been shown to suffer early embryonic lethality with non-beating hearts.[26] As the *TPM1 13_15del* variant is observed in heterozygosity in all individuals of the pedigree, this suggests the TPM1 heterodimeric assembly could exert dominant-negative effects to perturb wild-type (WT) TPM1 protein function.

CRISPR gene editing in *Xenopus* embryos

The early embryonic lethality of the *Tpm1* KO mouse embryos precluded the assessment of its role in ASD pathogenesis in mice. However, ASDs have been observed with *tpm1* morpholino (MO) gene knockdown (KD) in chick embryos.[27] To further assess experimentally how TPM1 deficiency may affect atrial septation, we conducted *tpm1* MO KD in *Xenopus laevis* embryos (Figures S2 and S3). *Xenopus* have three chamber hearts with distinct left and right atria, and *Xenopus* embryos can be obtained in large numbers and their development and viability can be visually tracked. We observed that 81% of the MO-injected *Xenopus laevis* embryos have severe pericardial edema, indicating heart failure with *tpm1* deficiency, and the heart rate was significantly reduced (Figures 3A and 3B). It should be noted that the *tpm1* gene is duplicated in *Xenopus leaveis*, and the two closely homologous *tpm1*-related genes are both targeted by the same MO used in these experiments (Figure S3). Similar analysis with *tpm1* gene KO generated by CRISPR-Cas9 gene editing replicated these findings in *X. tropicalis* embryos, with 64% of the CRISPR-targeted founder embryos exhibiting pericardial edema with reduced heart rate (Figures 3C and 3D). Analysis of the CRISPR-targeted embryos by western blotting confirmed the absence of TPM1 protein expression (Figure 3E). Histological reconstruction using episcopic confocal microscopy (ECM) showed large ASDs in some of the embryos after *tpm1* KD (*X. laevis*) or KO (*X. tropicalis*) (Figures 3F and S2D; Table S1).

Embryonic lethality with no heartbeat in *Tpm1* CRISPR-gene-edited mouse embryos

To further assess the functional effects of the $Tpm1^{K5del}$ mutation, we used CRISPR-Cas9 gene editing to pursue knock-in

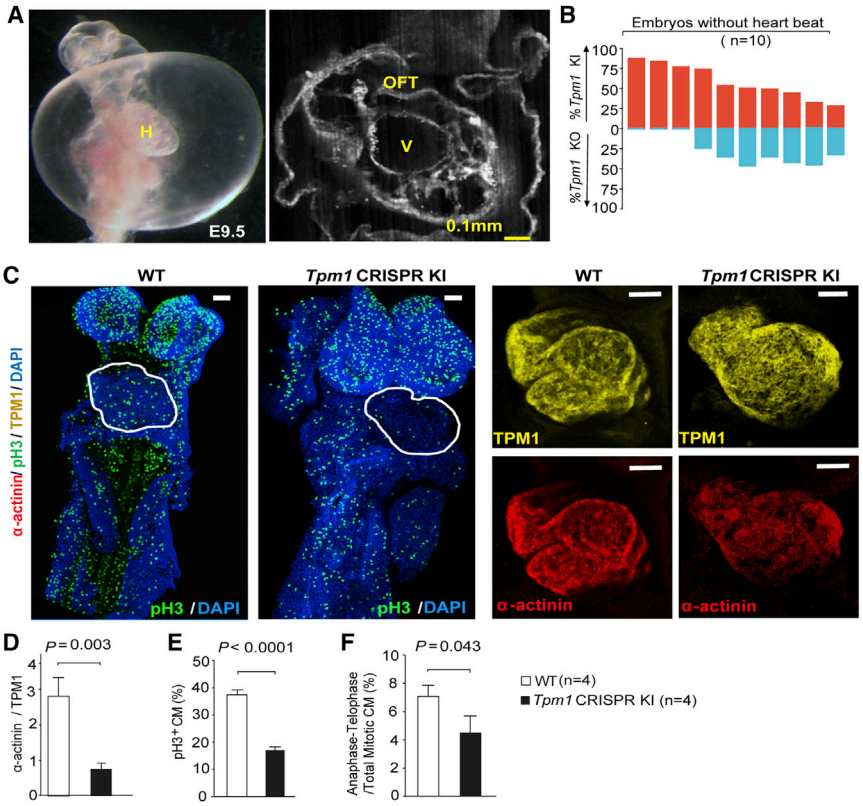

Figure 4. Severe pericardial effusion and early embryonic lethality of CRISPR *Tpm1* KI mouse embryos

(A) Representative example of E8.5 *Tpm1* CRISPR-Cas9 KI mouse embryo showed severe pericardial effusion with abnormal heart (H) looping seen in whole-mount view (left panel) and in a histological section (right panel) showing the outflow tract (OFT) and primitive ventricle (V) Scale bar, 0.1 mm.

(B) The frequency of *Tpm1* KI and KO in mouse embryos generated by CRISPR gene editing.

(C) Representative whole-mount confocal imaging of E8.5–9.0 WT and CRISPR-Cas9 *Tpm1* KI mouse embryos immunostained for TPM1, α-actinin, and phosphohistone H3. Scale bar, 500 μm.

(D–F) Quantitation of the ratio of α-actinin/TPM1 immunostaining (D), phosphohistone H3 (E), and ratio of anaphase-telophase per total mitotic cells (F) in the *Tpm1* KI versus WT control embryos (N > 2,000 cells).

In (B) and (D)–(F), the number of CRISPR mouse embryos analyzed in each experiment is indicated. Data for (D)–(F) are represented as mean ± SEM and analyzed using unpaired Student's t test.

(KI) of the *Tpm1* mutation in mice. Given the known lethality of the Tpm1 KO mouse, we conducted direct analysis of the CRISPR-gene-edited embryos referred to as founder embryo analyses. Mouse oocytes that were CRISPR targeted were transferred to surrogate mothers for development *in utero*, and noninvasive fetal ultrasound imaging was conducted daily from E7.5 onward to track embryo viability, growth, and development and to assess cardiac function. The number and viability of the embryos were recorded, and heart beating—which is initiated at E8.5—was tracked. We noted that embryos that failed to initiate heart beating at E8.5 were dead or resorbed by E9.5. This was observed for 64 of 67 *Tpm1* CRISPR-treated mouse embryos. (Table S2; Video S1). Whole-mount examination of these embryos harvested at E9.5 showed hydrops with severe pericardial effusion and abnormally looped heart tube (Figure 4A; Video S1). These results are reminiscent of those seen in the *Tpm1* KO mice that also showed no heartbeat with early embryonic lethality.[28]

K5del TPM1 exerts dominant-negative effects on WT TPM1 protein function

To assess the efficiency of CRISPR gene editing, E9.5 founder embryos were harvested, and DNA was extracted to assess the efficiency of CRISPR gene editing. The site of gene editing was PCR amplified and sequenced, and the Synthego Inference of CRISPR Edits (ICE) algorithm was used to analyze the sequencing data to determine the efficiency of CRISPR KI and KO events from nonhomologous end joining. This analysis revealed an average KI efficiency of 59%, with range of 28.2% to 98.9%, and an average KO of 21.6%, with range of 0% to 46% (Figure 4B; Table S3). In embryos with lower *Tpm1* KI efficiency, higher KO events were observed. As none of these embryos initiated heart beating, these findings would suggest the TPM1 K5del mutant protein can exert dominant-negative effects on WT TPM1 protein function. This is supported by observations from whole-mount embryo immunostaining of the CRISPR-targeted embryos for TPM1 and α-actinin protein expression (Figure 4C). This analysis showed TPM1 protein expression in the heart was preserved, while α-actinin expression was greatly reduced, resulting in the marked reduction (~73%) in the ratio of α-actinin/TPM1immunostaining (Figure 4D). Phosphohistone H3 staining of the same CRISPR-gene-edited embryos also showed a marked reduction in cell proliferation. This is specific to the heart, while noncardiac tissues of the embryo were unaffected (Figures 4C and 4E). This was accompanied by a reduction in mitotic cells at anaphase/telophase, indicating a delay or block in mitotic cell-cycle progression (Figure 4F). Together, these findings indicate the *Tpm1* mutation can exert dominant-negative effects to suppress normal TPM1 protein function.

Patient-induced pluripotent-stem-cell-derived CMs show mild defects

To assess the impact of the *TPM1* mutation on the patients, we generated induced pluripotent stem cells (iPSCs) from the index ASD subject (VI:1) and a healthy control subject and differentiated the iPSCs into cardiomyocytes (iPSC-CMs) using standard CM differentiation protocol. The efficiency of CM differentiation was unchanged, and the CMs generated were of normal size

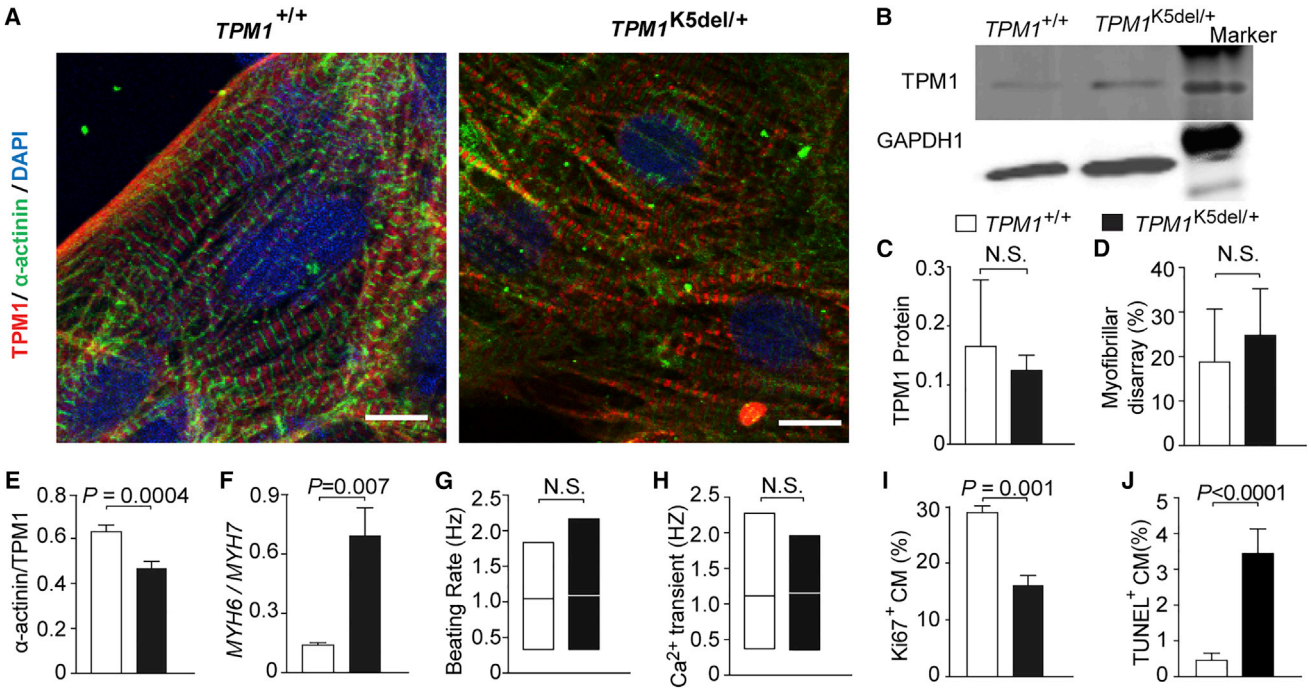

Figure 5. ASD patient iPSC-derived CM analysis

(A) Representative TPM1 and α-actinin immunostaining in control (left) and ASD (right) patient-derived iPSC-CMs showed similar TPM1 expression, but reduced expression of α-actinin. Reduction is observed in the ratio of α-actinin/TPM1 immunostaining intensity. Scale bar, 10 μm.

(B and C) Western blot of iPSC-CMs from WT control subject versus *TPM1*$^{K5del/+}$ ASD patient showed no change in TPM1 protein expression levels.

(D) Myofibrillar organization was unchanged in the *Tpm1* patient iPSC-CMs.

(E) Quantification showed the ratio of α-actinin to TPM1 was modestly decreased.

(F) *MYH6/MYH7* ratio in iPSC-CMs.

(G and H) Analysis of *TPM1*$^{K5del/+}$ iPSC-CMs showed no difference in beating rate (G) or calcium spark frequency (H), indicating preserved intrinsic contractility.

(I and J) Ki67 (I) and terminal deoxynucleotidyl transferase dUTP nick end labeling (TUNEL) labeling (J) in ASD patient and control iPSC-CMs.

Data for (C), (E), (F), (I), and (J) are represented as mean ± SEM and analyzed using unpaired Student's t test. Data for (G) and (H) are represented as boxplots with median and minimum-maximum shown and analyzed statistically using non-parametric Mann-Whitney test (two-tailed). The data for (C)–(J) are derived from three independent experiments. For (D), (E), (I), and (J), each experiment included analysis of >2000 iPSC-CMs.

with grossly normal myofilament organization (Figures 5A and S4). Western immunoblotting showed no change in the level of TPM1 protein expression compared to control (Figures 5B and 5C), and quantification of myofibrillar organization showed no evidence of myofibrillar disarray (Figure 5D). However, α-actinin expression was reduced (Figure 5A), resulting in lower α-actinin/TPM1 ratio (~20%) (Figure 5E). This change was relatively modest compared to the change observed in the *Tpm1* KI embryos (Figure 4D). The iPSC-CMs also showed marked alteration in the *MYH6/MYH7* transcript ratio that indicated a less mature differentiation state (Figure 5F). Functional assessments showed normal beating rate and calcium spark frequency (Figures 5G and 5H). Interestingly, cell proliferation was reduced, and apoptosis was increased, indicating the CMs generated from the patient-derived iPSCs were not entirely normal (Figures 5I and 5J). Nevertheless, the contractile function of the iPSC-CMs from the index ASD patient bearing the *TPM1*^{K5del} mutation appear to be preserved, consistent with the patient's long-term survival with grossly normal cardiac function. This contrasts with early embryonic lethality and failure to initiate heart beating in the *Tpm1* KI embryos.

Recovery of *TLN2* variant as a candidate protective variant

The rarity of the *TPM1*^{K5del} mutation in the human population is in line with the observed early embryonic lethality of the *Tpm1*^{K5del} mouse embryos. This is in striking contrast to the heritability of this mutation in eight members of the same extended family. This suggests buffering of the *TPM1*^{K5del} mutation by another variant in the genetic background of this family. To investigate this, we reanalyzed the WGS data using a less stringent frequency filter (MAF < 0.1), hypothesizing protective variants may be more common. Focusing on the same three chromosomal intervals coinherited by all eight ASD family members, we recovered 11 additional variants, of which 9 were found in proximity to the *TPM1*^{K5del} mutation (Data S1). Single-cell RNA sequencing data on human fetal hearts from 6.5 to 21 postconceptional weeks (PCWs) showed among the genes harboring the 11 candidate suppressor variants, only *TLN2* was co-expressed with *TPM1* in CMs (Figure 6A), making the heterozygous variant in *TLN2* (c.G6716A:p.R2239H;MAF = 0.01;CADD = 22.8) as the most likely suppressor gene (Figure 6B). *TLN2* is not only highly expressed in CMs, but it also plays a critical role in cardiac

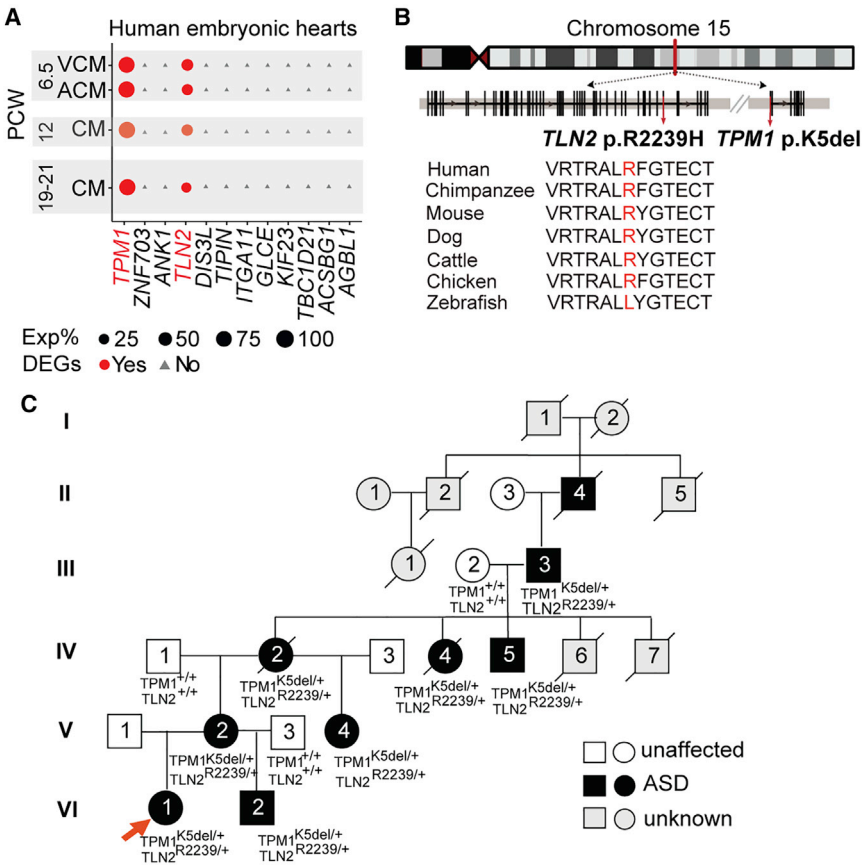

Figure 6. TLN2 variant is coinherited with the TPM1 mutation in the ASD family.

(A) Co-expression of *TPM1* and *TLN2* in CMs from human embryonic hearts at different postconceptional weeks (PCWs) gestation. Single-cell RNA sequencing data at 6.5, 12, and 19–21 PCW were obtained from Asp et al.,[30] Miao et al.,[31] and Suryawanshi et al.,[32] respectively. Dot size indicates percentage of cells expressing the indicated gene (Exp%). Genes and the corresponding dots are shown in red if they are differentially expressed in the indicated cell type. VCM, ventricular CM; ACM, atrial CM; DEGs, differentially expressed genes.

(B). The gene *TLN2* is situated on chromosome 15 close to *TPM1*. The *TLN2* variant recovered causes a R2239H missense mutation in a highly conserved amino acid residue situated within a conserved protein domain of TLN2.

(C) The $TPM1^{K5del/+}$ and $TLN2^{R2239H/+}$ mutations co-segregate with all subjects in the pedigree with ASDs. Lower right inset show sanger sequencing trace files of the *TLN2* variant recovered in the ASD family.

contractility. It encodes a large costameric protein bound to α-actinin and mediates extracellular matrix engagement by anchoring the actin myofilaments to integrins.[29] This *TLN2* variant was coinherited with the $TPM1^{K5del}$ mutation in all eight ASD subjects (Figure 6C), consistent with a possible role as a genetic modifier suppressing the severe deleterious effects of the *TPM1* mutation.

Tpm1/Tln2 KI cause ASDs with rescue of both heart beating and embryonic lethality

To functionally assess the *TLN2* (c.G6716A:p.R2239H) variant for a potential role in buffering the embryonic lethality of the $TPM1^{K5del}$ mutation, we conducted founder embryo analysis with mouse CRISPR-Cas9 double KI of the $Tpm1^{K5del}/Tln2^{R2239H}$ variants. Previous studies showed *Tln2* KO mice are viable with only mild late-onset skeletal myopathy.[29] We observed that with CRISPR *Tpm1/Tln2* double KI, 50% of the E8.5 embryos had beating hearts (27 of 56 embryos). This compares with only 4.4% of embryos with CRISPR gene editing directed at *Tpm1* alone (Table S2), yielding an OR of 19.35 (5.33–107.81, 95% CI) ($p = 9.63 \times 10^{-9}$) that indicated significant rescue of heart beating by the *Tln2* variant (Figure 7A).

To assess whether the rescued *Tpm1/Tln2* double-CRISPR-targeted embryos may have ASDs, 19 of these founder embryos were harvested at E16.5–17.5, the late-term stage when atrial septation is near complete, allowing for assessment of ASDs. This was conducted using 3D digital reconstructions of ECM-generated serial image stacks. It showed three of the double-targeted embryos had a large ASD (Figure 7B; Video S2). Double immunofluorescent staining for TPM1 and α-actinin showed normal sarcomere organization (Figure 7C). Quantification of the staining intensity showed TPM1 protein expression was unchanged, but α-actinin was decreased. This resulted in a modest reduction (~25%) in the α-actinin/TPM1 ratio, similar to the ASD patient iPSC-CMs, but markedly different from the severe depression observed in the *Tpm1* KI embryos (Figure 7C; compare to Figure 5C).

To quantitatively assess the KI efficiency in these 19 late-stage double-*Tpm1/Tln2*-CRISPR-targeted embryos, DNA was recovered from sections spanning the heart for analysis of CRISPR gene editing events. Analysis using the Synthego ICE algorithm to quantify the frequency of KI/KO events showed a paucity of *Tpm1* KI/KO events in these late-term fetuses, consistent with the early embryonic lethality with no heartbeat seen in the *Tpm1* KO/KI embryos. Only three embryos showed significant *Tpm1* KI events (56%–76%). These were also the three embryos found to have ASDs. Significantly, these three embryos also showed high levels of *Tln2* KI (81%–98%), supporting the role of the *Tln2* variant in suppression of the severe deleterious impact of the $Tpm1^{K5del}$ mutation (Figure 7D). These three embryos exhibited only low levels of KO events in *Tpm1* (2%–16%) and *Tln2* (0.82%–2%) (Table S4). In contrast, among the 16 embryos without ASDs, there was little or no *Tpm1* KI, but 5 had high levels of *Tpm1* KO (38%–57%). The latter embryos also showed significant levels of *Tln2* KI (30%–90%) (Figure 7D). Together, these findings support the role of *Tln2* in rescuing the embryonic lethality associated with *Tpm1* deficiency and with the rescue, uncovering the possible role of *Tpm1* in causing ASDs (Figure 7D; Table S4).

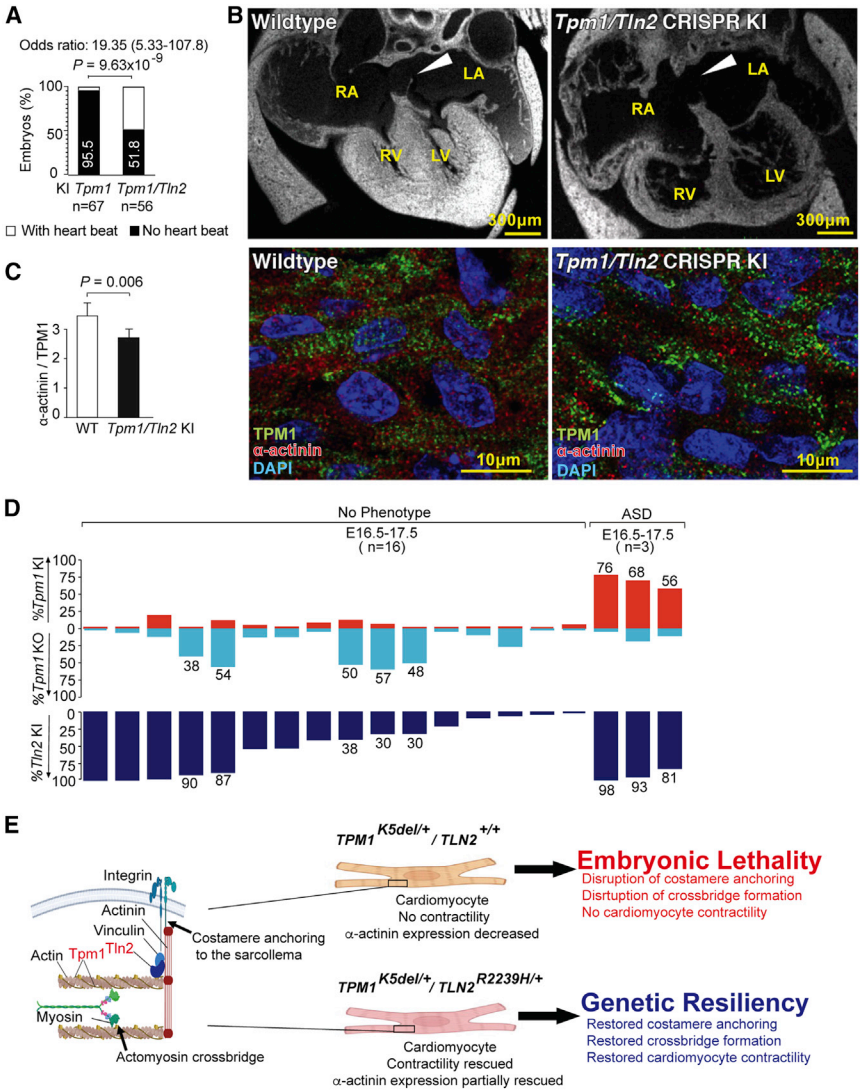

Figure 7. Rescue of *Tpm1* embryonic lethality and recapitulation of ASD in *Tpm1/Tln2* double-KI mice

(A) Significant rescue of heart beating was observed for the *Tpm1/Tln2* double-KI versus *Tpm1* KI mice. Some examples are shown in Video S1. n = number of embryos analyzed

(B) Representative histopathology and immunofluorescent staining of E16.5 *Tpm1/Tln2* double-KI verse WT mice hearts. Upper left panel shows normal atrial septum in a WT mouse embryo, while the upper right shows a large ASD in a CRISPR double-*Tpm1/Tln2*-KI embryo. Arrowhead points to atrial septum in the WT embryo, but this is not seen in the mutant double-KI embryo. The full 2D serial image stacks of these two hearts are shown in Video S2. Immunofluorescent staining of sections shows TPM1 and α-actinin expression in sarcomeric structures in the hearts of WT (left) and *Tpm1/Tln2*-double-KI (right) embryos. LV, left ventricle; RV, right ventricle.

(C) Quantification shows decreased α-actinin/TPM1 ratio in heart tissue of *Tpm1/Tln2*-double-KI (n = 3) versus WT embryos (n = 3).

(D) Efficiency of double *Tpm1/Tln2* KI in E16.5–17.5 embryos with or without ASDs. Note the ASD is only observed in embryos with effective *Tpm1/Tln2* double KI. n = number of embryos analyzed with or without ASD phenotype.

(E) Diagram showing TPM1 and TLN2 in the cardiac muscle and potential impact of the deleterious K5del *TPM1* mutation and its buffering by the *TLN2* variant.

Data for (A) were analyzed using Fisher's exact test. Data for (C), shown as means ± SEMs, were analyzed using unpaired Student's t test.

DISCUSSION

We identified an extremely rare pathogenic *TPM1 13_15del* mutation as the underlying cause for ASDs in a five-generation pedigree comprising eight individuals with ASD. This variant causing the deletion of an N-terminal lysine residue (p.K5del) is predicted to disrupt assembly of the α-helical coiled-coil dimer stabilizing actin filaments[24] and facilitating actomyosin cross-bridge formation (Figure 7E). As this perturbation would affect homodimers and heterodimers comprising mutant and WT proteins, dominant-negative effects would be expected that could contribute to disease. Consistent with this, our analysis of *Tpm1* CRISPR KI mouse embryos showed a severe defect in myofilament assembly. Thus, despite no change in TPM1 protein expression level, the *Tpm1* KI embryos showed a marked reduction in α-actinin and the ratio of α-actinin/TPM1 protein expression in the heart. These CRISPR *Tpm1* KI embryos also never initiated heart beating, a phenotype similar to that of the *Tpm1* KO mouse embryos. The pathogenicity of this *TPM1* mutation is supported by observation of an identical mutation in *TPM2*, a β-tropomyosin closely homologous to *TPM1* and known to cause rare autosomal dominant congenital skeletal myopathies.[33,34] The TPM2 mutant protein causes defects in actin myofilament assembly that are likely related to the disruption of head-to-tail β-tropomyosin polymerization.[34]

The rarity of the K5del *TPM1* mutation in the human population is likely accounted for by its dominant-negative effects blocking heartbeat initiation. While this mutation has been reported in only three individuals worldwide, its remarkable transmission in eight individuals of the same family over five generations suggested possible coinheritance of a protective genetic modifier. We identified this genetic modifier as a more common variant in *TLN2*, another sarcomeric actin-related gene coinherited with the *TPM1* mutation. *TLN2* is co-expressed with *TPM1* in embryonic and fetal CMs and is a component of the costamere structure anchoring sarcomeres to the membrane (Figure 7E). Significantly, double-CRISPR KI of the *Tpm1* and *Tln2* mutations in mice rescued heart beating and allowed survival with late-term fetuses also exhibiting ASDs. This was associated with the restoration of an α-actinin/Tpm1 ratio to more normal levels that are

similar to those observed in the beating iPSC-CMs derived from the index patient. Together, these findings suggest co-segregation of the *TLN2* variant underlies the high heritability of an otherwise rare embryonic lethal *TPM1* mutation. The *TLN2* variant may restore actomyosin cross-bridge formation and costamere anchoring, thus restoring CM contractility and heart beating (Figure 7E). The meiotic segregation of the *TLN2* suppressor variant from the embryonic lethal *TPM1 13_15del* mutation may explain the high incidence of miscarriages reported in this family.

TPM1 mutations have been associated with cases of hypertrophic cardiomyopathy (HCM) (5%) and DCM (1%–2%). Their role in ASDs has not been demonstrated but has been implicated by a screen for *TPM1* mutations in CHD patients.[35] However, the *c.13_15del* mutation was not recovered in this screen or in the screening of over 900 patients with CHDs in this study. Two other sarcomeric genes, *ACTC1* and *MYH6*, were previously identified to cause ASDs.[10,13–18] The role of the *TPM1 13_15del* mutation in ASDs was uncovered by suppression of its early embryonic lethality by the $TLN2^{G6716A}$ variant. Our finding of ASDs with *tpm1* CRISPR-mediated KO or MO KD in *Xenopus* embryos would suggest ASDs can arise from TPM1 deficiency. Although the mechanism for ASD pathogenesis is not well understood, the involvement of a cell proliferation defect is suggested by the reduced cell proliferation in the heart tissue of the *Tln2*/*Tpm1* double-CRISPR KI mouse embryo and in the iPSC-CMs of the index patient. It will be of interest to examine whether misoriented cell division planes may play a role, given this has been observed for ventricular septation defects.[36]

These findings provide a paradigm for how protective variants can increase genetic resiliency. Oligogenic inheritance of multiple pathogenic variants has been shown to cause CHDs[37,38] and cardiomyopathies.[39] While such studies showed multiple pathogenic variants can contribute to disease, our study showed pathogenic and protective variants in combination can provide the stable heritable transmission of an otherwise lethal mutation. It is worth noting that a study of genetic modifiers impacting ASD penetrance in heterozygous *Nkx2.5* KO mice indicated p13q in a heterogeneous population, and the predominant modifiers are likely to be suppressors buffering against the pathogenic mutations.[19] Together, these findings raise the possibility that protective and pathogenic variants interact in oligogenic combinations to contribute to the complex genetics of human CHDs.

In summary, our study identified a critical role for a severe lethal *TPM1* mutation in the genetic etiology of ASDs. Importantly, we further showed emergence of the ASD phenotype was made possible by the coinheritance of a protective variant suppressing the embryonic lethality of the pathogenic *TPM1* mutation. These findings provide a paradigm for how individuals harboring severe disease-causing mutations can be without disease.[2] Our findings also indicate the possible use of founder mouse modeling with CRISPR gene editing to assess variant pathogenicity. Not requiring the breeding of mice, the founder analysis is rapid and cost effective and can accelerate the testing of variant contribution to human disease. This may be especially critical for variants likely to cause dominant embryonic lethal phenotypes difficult to functionally assess otherwise, as demonstrated by the K5del *TPM1* mutation. Based on the American College of Medical Genetics criteria for variant classification,[40] our familial segregation analysis and functional studies with patient iPSCs and animal modeling would support reclassification of the K5del *TPM1* variant from VUS to likely pathogenic.

Limitations of the study

There are several limitations in our study to note. One relates to the animal modeling for assessing the biological impact of the *TPM1* variant. The mouse CRISPR gene editing showed the *Tpm1* mutation causes embryonic lethality associated with a lack of heart beating, but *tpm1* MO KD or KO in *Xenopus* embryos caused marked reduction but not extinction of heart beating. This difference could reflect species differences. Alternatively, *Xenopus*, unlike mice, are not inbred. Thus, genetic modifiers in its heterogeneous genetic background may provide more robust rescue of *tpm1*-dependent sarcomere function. Second, we tested only one variant for suppressor function, the *TLN2* variant. We note *TLN2* is the only candidate gene from the linkage interval expressed in the embryonic heart, other than *TPM1*, and both genes functionally converge on the regulation of sarcomeric actin. In addition, strong support for the *Tln2* variant acting as a suppressor can be seen in the significant rescue of heart beating in mouse embryos with *Tpm1*/*Tln2* double KI, but not with *Tpm1* KI alone. However, *TLN2* suppressor function in the human context will need to be further investigated with CRISPR correction of the *TLN2* variant in the patient iPSCs and examining its impact on iPSC-CM contractility, analyses beyond the scope of the present study. A third limitation is the discrepant finding of three unrelated individuals with the *TPM1* pathogenic variant but without ASDs. As these are the only three individuals worldwide with the *TPM1* mutation outside of the ASD pedigree, these are ultra-rare individuals that may have fortuitously coinherited multiple suppressor mutations, allowing more robust suppression of the pathogenic effects of the *TPM1* mutation. Finally, another limitation is the fact that CRISPR mouse modeling with *TPM1*/*TLN2* double KI yielded ASDs in only 3 of 19 late-term fetuses. However, we note all three fetuses with ASDs had substantial *TPM1* (>50%) KI, supporting its role in ASD pathogenesis. Additionally, all three fetuses also showed high-level *Tln2* KI, consistent with the role of *Tln2* in suppression of the early embryonic lethality of the K5del *Tpm1* variant. Overall, these limitations do not detract from the main conclusion that genetic resiliency can arise from genetic suppression of a deleterious mutation, findings that suggest both pathogenic and protective variants contribute to the genetic architecture of human diseases.

STAR★METHODS

Detailed methods are provided in the online version of this paper and include the following:

- KEY RESOURCES TABLE
- RESOURCE AVAILABILITY
  - Lead contact
  - Materials availability
  - Data and code availability

SUPPLEMENTAL INFORMATION

Supplemental information can be found online at https://doi.org/10.1016/j.xcrm.2021.100501.

ACKNOWLEDGMENTS

We are truly indebted to all family members for their research participation and contribution to this project. We thank H. Yagi, A. Engel, and C. Heffner for technical assistance. This work was supported by NIH grants HL132024, HL142788 (C.W.L.), and R01HL036153 (W.J.L.); UPMC Fellows Grant (P.T., X.X.); the Research Grants Council of Hong Kong 14167017 and 14112618 (H.Z.); and American Heart Association/Children's Heart Foundation fellowship (X.X.). Additional support was provided by the Centre for Cardiovascular Genomics and Medicine, Lui Che Woo Institute of Innovative Medicine, The Chinese University of Hong Kong (P.T.).

AUTHOR CONTRIBUTIONS

Study design, P.T., W.Z., X.X., C.B.Y., and C.W.L.; recruitment of research participants, sample collection, clinical data curation, P.T., M.Z., T.C.W., F.A., J.-h.L., M.-L.F., B.K., E.F., B.F., and C.W.L.; WGS and linkage analysis, W.Z., H.G., and A.S.B.; single-cell RNA sequencing analysis, W.Z.; iPSC modeling, X.X.; CM analysis, X.X., C.B.Y., and T.F.; *Xenopus* MO and CRISPR/Cas9 experiments, A.M.S., S.M.W., C.W., and H.Z; mouse CRISPR experiments, K.A.P., S.M., Y.S., and K.O.; mouse ultrasound phenotyping, T.T.; Sanger sequencing and genotyping, P.T., A.M.B., E.F., G.T., T.-P.A., M.X.W., and B.J.G.; imaging analysis, P.T., X.X., C.B.Y., S.H.,Y.L.W., G.C.G., and D.A.S.; molecular modeling, W.J.L. and M.J.R.; statistics, P.T. and C.W.L.; manuscript preparation, C.W.L., P.T., W.Z., X.X., C.B.Y., and G.C.G.

DECLARATION OF INTERESTS

The authors declare no competing interests.

Received: May 15, 2021
Revised: October 24, 2021
Accepted: December 17, 2021
Published: January 28, 2022

REFERENCES

1. Boycott, K.M., Vanstone, M.R., Bulman, D.E., and MacKenzie, A.E. (2013). Rare-disease genetics in the era of next-generation sequencing: discovery to translation. Nat. Rev. Genet. *14*, 681–691. https://doi.org/10.1038/nrg3555.
2. Chen, R., Shi, L., Hakenberg, J., Naughton, B., Sklar, P., Zhang, J., Zhou, H., Tian, L., Prakash, O., Lemire, M., et al. (2016). Analysis of 589,306 genomes identifies individuals resilient to severe Mendelian childhood diseases. Nat. Biotechnol. *34*, 531–538. https://doi.org/10.1038/nbt.3514.
3. Ferencz, C., Rubin, J.D., McCarter, R.J., Brenner, J.I., Neill, C.A., Perry, L.W., Hepner, S.I., and Downing, J.W. (1985). Congenital heart disease: prevalence at livebirth. The Baltimore-Washington Infant Study. Am. J. Epidemiol. *121*, 31–36. https://doi.org/10.1093/oxfordjournals.aje.a113979.
4. Hoffman, J.I., and Kaplan, S. (2002). The incidence of congenital heart disease. J. Am. Coll. Cardiol. *39*, 1890–1900. https://doi.org/10.1016/s0735-1097(02)01886-7.
5. Botto, L.D., Correa, A., and Erickson, J.D. (2001). Racial and temporal variations in the prevalence of heart defects. Pediatrics *107*, E32. https://doi.org/10.1542/peds.107.3.e32.
6. Marelli, A.J., Mackie, A.S., Ionescu-Ittu, R., Rahme, E., and Pilote, L. (2007). Congenital heart disease in the general population: changing prevalence and age distribution. Circulation *115*, 163–172. https://doi.org/10.1161/CIRCULATIONAHA.106.627224.
7. Emerit, I., de Grouchy, J., Vernant, P., and Corone, P. (1967). Chromosomal abnormalities and congenital heart disease. Circulation *36*, 886–905. https://doi.org/10.1161/01.cir.36.6.886.
8. Noonan, J.A. (1978). Association of congenital heart disease with syndromes or other defects. Pediatr. Clin. North Am. *25*, 797–816. https://doi.org/10.1016/s0031-3955(16)33643-4.
9. Zetterqvist, P. (1960). Multiple occurrence of atrial septal defect in a family. Acta Paediatr. (Stockh.) *49*, 741–747. https://doi.org/10.1111/j.1651-2227.1960.tb16081.x.
10. Posch, M.G., Perrot, A., Berger, F., and Ozcelik, C. (2010). Molecular genetics of congenital atrial septal defects. Clin. Res. Cardiol. *99*, 137–147. https://doi.org/10.1007/s00392-009-0095-0.
11. Nora, J.J., McNamara, D.G., and Fraser, F.C. (1967). Hereditary factors in atrial septal defect. Circulation *35*, 448–456. https://doi.org/10.1161/01.cir.35.3.448.
12. Schott, J.J., Benson, D.W., Basson, C.T., Pease, W., Silberbach, G.M., Moak, J.P., Maron, B.J., Seidman, C.E., and Seidman, J.G. (1998). Congenital heart disease caused by mutations in the transcription factor NKX2-5. Science *281*, 108–111. https://doi.org/10.1126/science.281.5373.108.
13. Ching, Y.H., Ghosh, T.K., Cross, S.J., Packham, E.A., Honeyman, L., Loughna, S., Robinson, T.E., Dearlove, A.M., Ribas, G., Bonser, A.J., et al. (2005). Mutation in myosin heavy chain 6 causes atrial septal defect. Nat. Genet. *37*, 423–428. https://doi.org/10.1038/ng1526.
14. Matsson, H., Eason, J., Bookwalter, C.S., Klar, J., Gustavsson, P., Sunnegårdh, J., Enell, H., Jonzon, A., Vikkula, M., Gutierrez, I., et al. (2008). Alpha-cardiac actin mutations produce atrial septal defects. Hum. Mol. Genet. *17*, 256–265. https://doi.org/10.1093/hmg/ddm302.
15. McNally, E., and Dellefave, L. (2009). Sarcomere mutations in cardiogenesis and ventricular noncompaction. Trends Cardiovasc. Med. *19*, 17–21. https://doi.org/10.1016/j.tcm.2009.03.003.
16. Budde, B.S., Binner, P., Waldmüller, S., Höhne, W., Blankenfeldt, W., Hassfeld, S., Brömsen, J., Dermintzoglou, A., Wieczorek, M., May, E., et al. (2007). Noncompaction of the ventricular myocardium is associated

with a de novo mutation in the beta-myosin heavy chain gene. PLoS ONE *2*, e1362. https://doi.org/10.1371/journal.pone.0001362.

17. Garg, V., Kathiriya, I.S., Barnes, R., Schluterman, M.K., King, I.N., Butler, C.A., Rothrock, C.R., Eapen, R.S., Hirayama-Yamada, K., Joo, K., et al. (2003). GATA4 mutations cause human congenital heart defects and reveal an interaction with TBX5. Nature *424*, 443–447. https://doi.org/10.1038/nature01827.
18. Khan, R., and Jay, P.Y. (2015). Human genetics of atrial septal defect. Congenital Heart Diseases: The Broken Heart: Clinical Features, Human Genetics and Molecular Pathways (Springer-Verlag), pp. 279–290.
19. Winston, J.B., Erlich, J.M., Green, C.A., Aluko, A., Kaiser, K.A., Takematsu, M., Barlow, R.S., Sureka, A.O., LaPage, M.J., Janss, L.L., and Jay, P.Y. (2010). Heterogeneity of genetic modifiers ensures normal cardiac development. Circulation *121*, 1313–1321. https://doi.org/10.1161/CIRCULATIONAHA.109.887687.
20. Santos, R., Kawauchi, S., Jacobs, R.E., Lopez-Burks, M.E., Choi, H., Wikenheiser, J., Hallgrimsson, B., Jamniczky, H.A., Fraser, S.E., Lander, A.D., and Calof, A.L. (2016). Conditional Creation and Rescue of Nipbl-Deficiency in Mice Reveals Multiple Determinants of Risk for Congenital Heart Defects. PLoS Biol. *14*, e2000197. https://doi.org/10.1371/journal.pbio.2000197.
21. Kirk, E.P., Hyun, C., Thomson, P.C., Lai, D., Castro, M.L., Biben, C., Buckley, M.F., Martin, I.C., Moran, C., and Harvey, R.P. (2006). Quantitative trait loci modifying cardiac atrial septal morphology and risk of patent foramen ovale in the mouse. Circ. Res. *98*, 651–658. https://doi.org/10.1161/01.RES.0000209965.59312.aa.
22. Flaquer, A., Baumbach, C., Piñero, E., García Algas, F., de la Fuente Sanchez, M.A., Rosell, J., Toquero, J., Alonso-Pulpon, L., Garcia-Pavia, P., Strauch, K., and Heine-Suñer, D. (2013). Genome-wide linkage analysis of congenital heart defects using MOD score analysis identifies two novel loci. BMC Genet. *14*, 44. https://doi.org/10.1186/1471-2156-14-44.
23. Schultheiss, T., Lin, Z.X., Lu, M.H., Murray, J., Fischman, D.A., Weber, K., Masaki, T., Imamura, M., and Holtzer, H. (1990). Differential distribution of subsets of myofibrillar proteins in cardiac nonstriated and striated myofibrils. J. Cell Biol. *110*, 1159–1172. https://doi.org/10.1083/jcb.110.4.1159.
24. Hitchcock-DeGregori, S.E. (2008). Tropomyosin: function follows structure. Adv. Exp. Med. Biol. *644*, 60–72. https://doi.org/10.1007/978-0-387-85766-4_5.
25. Teekakirikul, P., Padera, R.F., Seidman, J.G., and Seidman, C.E. (2012). Hypertrophic cardiomyopathy: translating cellular cross talk into therapeutics. J. Cell Biol. *199*, 417–421. https://doi.org/10.1083/jcb.201207033.
26. McKeown, C.R., Nowak, R.B., Gokhin, D.S., and Fowler, V.M. (2014). Tropomyosin is required for cardiac morphogenesis, myofibril assembly, and formation of adherens junctions in the developing mouse embryo. Dev. Dyn. *243*, 800–817. https://doi.org/10.1002/dvdy.24115.
27. England, J., Granados-Riveron, J., Polo-Parada, L., Kuriakose, D., Moore, C., Brook, J.D., Rutland, C.S., Setchfield, K., Gell, C., Ghosh, T.K., et al. (2017). Tropomyosin 1: Multiple roles in the developing heart and in the formation of congenital heart defects. J. Mol. Cell. Cardiol. *106*, 1–13. https://doi.org/10.1016/j.yjmcc.2017.03.006.
28. Blanchard, E.M., Iizuka, K., Christe, M., Conner, D.A., Geisterfer-Lowrance, A., Schoen, F.J., Maughan, D.W., Seidman, C.E., and Seidman, J.G. (1997). Targeted ablation of the murine alpha-tropomyosin gene. Circ. Res. *81*, 1005–1010. https://doi.org/10.1161/01.res.81.6.1005.
29. Manso, A.M., Okada, H., Sakamoto, F.M., Moreno, E., Monkley, S.J., Li, R., Critchley, D.R., and Ross, R.S. (2017). Loss of mouse cardiomyocyte talin-1 and talin-2 leads to β-1 integrin reduction, costameric instability, and dilated cardiomyopathy. Proc. Natl. Acad. Sci. USA *114*, E6250–E6259. https://doi.org/10.1073/pnas.1701416114.
30. Asp, M., Giacomello, S., Larsson, L., Wu, C., Furth, D., Qian, X., Wardell, E., Custodio, J., Reimegard, J., Salmen, F., et al. (2019). A Spatiotemporal Organ-Wide Gene Expression and Cell Atlas of the Developing Human Heart. Cell *179*, 1647–1660.e1619. https://doi.org/10.1016/j.cell.2019.11.025.
31. Miao, Y., Tian, L., Martin, M., Paige, S.L., Galdos, F.X., Li, J., Klein, A., Zhang, H., Ma, N., Wei, Y., et al. (2020). Intrinsic Endocardial Defects Contribute to Hypoplastic Left Heart Syndrome. Cell Stem Cell *27*, 574–589.e8. https://doi.org/10.1016/j.stem.2020.07.015.
32. Suryawanshi, H., Clancy, R., Morozov, P., Halushka, M.K., Buyon, J.P., and Tuschl, T. (2020). Cell atlas of the foetal human heart and implications for autoimmune-mediated congenital heart block. Cardiovasc. Res. *116*, 1446–1457. https://doi.org/10.1093/cvr/cvz257.
33. Marttila, M., Lehtokari, V.L., Marston, S., Nyman, T.A., Barnerias, C., Beggs, A.H., Bertini, E., Ceyhan-Birsoy, O., Cintas, P., Gerard, M., et al. (2014). Mutation update and genotype-phenotype correlations of novel and previously described mutations in TPM2 and TPM3 causing congenital myopathies. Hum. Mutat. *35*, 779–790. https://doi.org/10.1002/humu.22554.
34. Davidson, A.E., Siddiqui, F.M., Lopez, M.A., Lunt, P., Carlson, H.A., Moore, B.E., Love, S., Born, D.E., Roper, H., Majumdar, A., et al. (2013). Novel deletion of lysine 7 expands the clinical, histopathological and genetic spectrum of TPM2-related myopathies. Brain *136*, 508–521. https://doi.org/10.1093/brain/aws344.
35. Teekakirikul, P., Kelly, M.A., Rehm, H.L., Lakdawala, N.K., and Funke, B.H. (2013). Inherited cardiomyopathies: molecular genetics and clinical genetic testing in the postgenomic era. J. Mol. Diagn. *15*, 158–170. https://doi.org/10.1016/j.jmoldx.2012.09.002.
36. Chen, C.T., Hehnly, H., Yu, Q., Farkas, D., Zheng, G., Redick, S.D., Hung, H.F., Samtani, R., Jurczyk, A., Akbarian, S., et al. (2014). A unique set of centrosome proteins requires pericentrin for spindle-pole localization and spindle orientation. Curr. Biol. *24*, 2327–2334. https://doi.org/10.1016/j.cub.2014.08.029.
37. Gifford, C.A., Ranade, S.S., Samarakoon, R., Salunga, H.T., de Soysa, T.Y., Huang, Y., Zhou, P., Elfenbein, A., Wyman, S.K., Bui, Y.K., et al. (2019). Oligogenic inheritance of a human heart disease involving a genetic modifier. Science *364*, 865–870. https://doi.org/10.1126/science.aat5056.
38. Liu, X., Yagi, H., Saeed, S., Bais, A.S., Gabriel, G.C., Chen, Z., Peterson, K.A., Li, Y., Schwartz, M.C., Reynolds, W.T., et al. (2017). The complex genetics of hypoplastic left heart syndrome. Nat. Genet. *49*, 1152–1159. https://doi.org/10.1038/ng.3870.
39. Ren, M.B., Chai, X.R., Li, L., Wang, X., and Yin, C. (2020). Potential digenic inheritance of familial hypertrophic cardiomyopathy identified by whole-exome sequencing. Mol. Genet. Genomic Med. *8*, e1150. https://doi.org/10.1002/mgg3.1150.
40. Richards, S., Aziz, N., Bale, S., Bick, D., Das, S., Gastier-Foster, J., Grody, W.W., Hegde, M., Lyon, E., Spector, E., et al.; ACMG Laboratory Quality Assurance Committee (2015). Standards and guidelines for the interpretation of sequence variants: a joint consensus recommendation of the American College of Medical Genetics and Genomics and the Association for Molecular Pathology. Genet. Med. *17*, 405–424. https://doi.org/10.1038/gim.2015.30.
41. Sander, J.D., Dahlborg, E.J., Goodwin, M.J., Cade, L., Zhang, F., Cifuentes, D., et al. (2011). Selection-free zinc-finger-nuclease engineering by context-dependent assembly (CoDA). Nat. Methods *8*, 67–69.
42. Liu, X., Tobita, K., Francis, R.J., and Lo, C.W. (2013). Imaging techniques for visualizing and phenotyping congenital heart defects in murine models. Birth Defects Res. C Embryo Today *99*, 93–105. https://doi.org/10.1002/bdrc.21037.
43. Abecasis, G.R., Cherny, S.S., Cookson, W.O., and Cardon, L.R. (2002). Merlin–rapid analysis of dense genetic maps using sparse gene flow trees. Nat. Genet. *30*, 97–101. https://doi.org/10.1038/ng786.
44. Li, H., and Durbin, R. (2010). Fast and accurate long-read alignment with Burrows-Wheeler transform. Bioinformatics *26*, 589–595.
45. Van der Auwera, G.A., Carneiro, M.O., Hartl, C., Poplin, R., Del Angel, G., Levy-Moonshine, A., Jordan, T., Shakir, K., Roazen, D., Thibault, J., et al. (2013). From FastQ data to high confidence variant calls: the Genome

Analysis Toolkit best practices pipeline. Curr. Protoc. Bioinformatics *43*, 11.10.11–11.10.33. https://doi.org/10.1002/0471250953.bi1110s43.

46. Wang, K., Li, M., and Hakonarson, H. (2010). ANNOVAR: functional annotation of genetic variants from high-throughput sequencing data. Nucleic Acids Res. *38*, e164. https://doi.org/10.1093/nar/gkq603.
47. Abyzov, A., Urban, A.E., Snyder, M., and Gerstein, M. (2011). CNVnator: an approach to discover, genotype, and characterize typical and atypical CNVs from family and population genome sequencing. Genome Res. *21*, 974–984. https://doi.org/10.1101/gr.114876.110.
48. Chen, K., Wallis, J.W., McLellan, M.D., Larson, D.E., Kalicki, J.M., Pohl, C.S., et al. (2009). BreakDancer: an algorithm for high-resolution mapping of genomic structural variation. Nat. Methods *6*, 677–681.
49. Butler, A., Hoffman, P., Smibert, P., Papalexi, E., and Satija, R. (2018). Integrating single-cell transcriptomic data across different conditions, technologies, and species. Nat. Biotechnol. *36*, 411–420. https://doi.org/10.1038/nbt.4096.
50. Cordell, H.J., Bentham, J., Topf, A., Zelenika, D., Heath, S., Mamasoula, C., Cosgrove, C., Blue, G., Granados-Riveron, J., Setchfield, K., et al. (2013). Genome-wide association study of multiple congenital heart disease phenotypes identifies a susceptibility locus for atrial septal defect at chromosome 4p16. Nat. Genet. *45*, 822–824. https://doi.org/10.1038/ng.2637.
51. Xu, X., Tan, T., Ivy Lin, J.-H., Adams, P., Liu, X., Feinstein, T.N., Khalifa, O., Porter, G.A., Shiva, S.S., and Lo, C. (2018). Intrinsic Cardiomyocyte Mitochondrial Defects Underlie Cardiac Dysfunction and Heart Failure Risk Associated with Hypoplastic Left Heart Syndrome. Circulation *138*, A15746.
52. Xu, X., Jin, K., Bais, A.S., Zhu, W., Yagi, H., Feinstein, T.N., Nguyen, P., Criscione, J., Liu, X., Beutner, G., et al. (2021). iPSC modeling shows uncompensated mitochondrial mediated oxidative stress underlies early heart failure in hypoplastic left heart syndrome. bioRxiv. https://doi.org/10.1101/2021.05.09.443165.
53. Li, H., and Durbin, R. (2010). Fast and accurate long-read alignment with Burrows-Wheeler transform. Bioinformatics *26*, 589–595. https://doi.org/10.1093/bioinformatics/btp698.
54. Fan, X., Abbott, T.E., Larson, D., and Chen, K. (2014). BreakDancer: Identification of Genomic Structural Variation from Paired-End Read Mapping. Curr. Protoc. Bioinformatics *45*, 15.16.1–15.16.11. https://doi.org/10.1002/0471250953.bi1506s45.
55. Karczewski, K.J., Francioli, L.C., Tiao, G., Cummings, B.B., Alföldi, J., Wang, Q., Collins, R.L., Laricchia, K.M., Ganna, A., Birnbaum, D.P., et al.; Genome Aggregation Database Consortium (2020). The mutational constraint spectrum quantified from variation in 141,456 humans. Nature *581*, 434–443. https://doi.org/10.1038/s41586-020-2308-7.
56. Liu, X., Wu, C., Li, C., and Boerwinkle, E. (2016). dbNSFP v3.0: A One-Stop Database of Functional Predictions and Annotations for Human Nonsynonymous and Splice-Site SNVs. Hum. Mutat. *37*, 235–241. https://doi.org/10.1002/humu.22932.
57. Liu, Z., Cheng, T.T., Shi, Z., Liu, Z., Lei, Y., Wang, C., Shi, W., Chen, X., Qi, X., Cai, D., et al. (2016). Efficient genome editing of genes involved in neural crest development using the CRISPR/Cas9 system in Xenopus embryos. Cell Biosci. *6*, 22. https://doi.org/10.1186/s13578-016-0088-4.
58. Liu, X., Francis, R., Kim, A.J., Ramirez, R., Chen, G., Subramanian, R., Anderton, S., Kim, Y., Wong, L., Morgan, J., et al. (2014). Interrogating congenital heart defects with noninvasive fetal echocardiography in a mouse forward genetic screen. Circ. Cardiovasc. Imaging *7*, 31–42. https://doi.org/10.1161/CIRCIMAGING.113.000451.
59. Hsiau, T., Conant, D., Rossi, N., Maures, T., Waite, K., Yang, J., Joshi, S., Kelso, R., Holden, K., Enzmann, B.L., and Stoner, R. (2019). Inference of CRISPR Edits from Sanger Trace Data. bioRxiv. https://doi.org/10.1101/251082.
60. Schneider, C.A., Rasband, W.S., and Eliceiri, K.W. (2012). NIH Image to ImageJ: 25 years of image analysis. Nat. Methods *9*, 671–675. https://doi.org/10.1038/nmeth.2089.
61. Okita, K., Matsumura, Y., Sato, Y., Okada, A., Morizane, A., Okamoto, S., Hong, H., Nakagawa, M., Tanabe, K., Tezuka, K., et al. (2011). A more efficient method to generate integration-free human iPS cells. Nat. Methods *8*, 409–412. https://doi.org/10.1038/nmeth.1591.
62. Xu, X., Wang, Q., Long, Y., Zhang, R., Wei, X., Xing, M., Gu, H., and Xie, X. (2013). Stress-mediated p38 activation promotes somatic cell reprogramming. Cell Res. *23*, 131–141. https://doi.org/10.1038/cr.2012.143.
63. Burridge, P.W., Matsa, E., Shukla, P., Lin, Z.C., Churko, J.M., Ebert, A.D., Lan, F., Diecke, S., Huber, B., Mordwinkin, N.M., et al. (2014). Chemically defined generation of human cardiomyocytes. Nat. Methods *11*, 855–860. https://doi.org/10.1038/nMeth.2999.

STAR★METHODS

KEY RESOURCES TABLE

REAGENT or RESOURCE	SOURCE	IDENTIFIER
Antibodies		
TPM1 Antibody	Abcam	Cat# ab55915; RRID:AB_883154
Anti-Sarcomeric Alpha Actinin antibody	Sigma-Aldrich	Cat# A7811; RRID:AB_476766
pH3	Millipore	Cat#06-570; RRID: AB_310177
AF555 goat anti-rabbit IgG	ThermoFisher	Cat# A-21428; RRID:AB_2535849
AF647 goat anti-mouse IgG1	ThermoFisher	Cat# A-21240; RRID:AB_2535809
Anti-Sarcomeric Alpha Actinin antibody	abcam	RRID:AB_137346
ki67	Abcam	Cat# ab15580; RRID:AB_443209
human iPSC-CM: goat anti-rabbit IgG	ThermoFisher	Cat# A-21429; RRID:AB_2535850
human iPSC-CM: goat anti-mouse IgM	ThermoFisher	Cat# A-21042; RRID:AB_2535711
TroponinT, Cardiac Isoform Ab-1, Mouse Monoclonal Antibody	Lab Vision	Cat# MS-295-P1; RRID:AB_61808
ph3Anti-HistoneH3 (phosphoS10) antibody [mAbcam14955] (AlexaFluor®488)	abcam	Cat# ab14955; RRID:AB_443110
Chemicals, peptides, and recombinant proteins		
Alt-R S.p. Cas9 Nuclease 3NLS	Integrated DNA Techonologies	RRID: #1074181
Critical commercial assays		
e-Mycoplus Mycoplasma PCR DetectionKit	bocascientific	25235
Matrigel® hESC-Qualified Matrix, *LDEV-free	Corning	354277
mTeSR	STEMCELL Technologies	85850
Nucleofector Kits for Human Dermal Fibroblast (NHDF)	Lonza	VPD-1001
RPMI 1640 Medium, noglucose	Thermofisher	11879020
KSOM medium	Millipore	#MR-121-D
DNA extraction kit—QIAamp DNA FFPE tissue kit	QIAGEN	#56404
RNA extraction kit-Trizol reagent	Invitrogen	#12183555
MAXIscript T7 transcription kit	ThermoFisher	#AM1312
TUNEL assay kit	Sigma Millipore	#12156792910 Roche
Deposited data		
Raw sequencing reads of WGS and genotype data of SNP Array	This paper	PRJNA624983
Single cell RNA sequencing data at 6.5 PCW	Asp et al.[30]	https://www.spatialresearch.org/resources-published-datasets/doi-10-1016-j-cell-2019-11-025/
Single cell RNA sequencing data at 12 PCW	Miao et al.[31]	Single Cell Portal: SCP1021
Single cell RNA sequencing data at 19-21 PCW	Suryawanshi et al.[32]	PRJNA576243
Experimental models: Cell lines		
iPSC-CM from patient with ASD and healthy subject	This paper	N/A
Experimental models: Organisms/strains		
B6D2F1 strain mouse	Jackson Laboratory	100006
CD1 strain mouse	Jackson Laboratory	003814
X. laevis Xenopus	Chinese University of Hong Kong and Indiana University School	N/A
X. tropicalis Xenopus	Chinese University of Hong Kong and Indiana University School	N/A

(*Continued on next page*)

Continued

REAGENT or RESOURCE	SOURCE	IDENTIFIER
Oligonucleotides		
Human *TPM1* primers for variant confirmation Forward: GTCATATCCACCGTCAACTGG	This paper	N/A
Human *TPM1* primers for variant confirmation Reverse: ACCTGCTTGCTCCTGTCTTC	This paper	N/A
Human *TLN2* primers for variant confirmation Forward: GAGTCTGGGACTGCCCAAT	This paper	N/A
Human *TLN2* primers for variant confirmation Reverse: CCAGGACAGCTAGAGGGACA	This paper	N/A
Mouse *Tpm1* Primers for mouse CRISPR genotyping Forward: TCCTAAGGAATGCGGTCGCCC	This paper	N/A
Mouse *Tpm1* Primers for mouse CRISPR genotyping Reverse: AGTCAGAGAAGGGCCACGAGC	This paper	N/A
Mouse *Tln2* Primers for mouse CRISPR genotyping Forward: AGACCAGAGTACCCAGCACTGC	This paper	N/A
Mouse *Tln2* Primers for mouse CRISPR genotyping Reverse: CCCAGGCGTGTTCTTTCTGCC	This paper	N/A
X.tropicalis Tpm1 CRISPR target region genotyping Forward: CCCAGGGCTCAGACTAGGAA	This paper	N/A
X.tropicalis Tpm1 CRISPR target region genotyping Reverse: TTGAGACAGGTCCTTGGGGG	This paper	N/A
X.laevis Tpm1 Morpholino oligo sequence: CATCTTCTTCTTGATGGCGTCCATG	This paper	N/A
X.tropicalis *Tpm1* CRISPR sgRNA 1 Forward: TAGGCCTTGGACAGAGCAGAAC	This paper	N/A
X.tropicalis *Tpm1* CRISPR sgRNA 1 Reverse: AAACGTTCTGCTCTGTCCAAGG	This paper	N/A
Mouse *Tpm1* CRISPR sgRNA: CTTCTTGATGGCGTCCATGG	This paper	N/A
Mouse *Tpm1* CRISPR single-stranded donor: TCCGCTGCCTAAG GGCCCCTCGCCACCGCCACCATGGACGCCATC AAGAAGATGCAGATGCTGAAGCTCGACAAAGAGAACG CCTTGGATCGAGCTGAGCAAGCGGAGGCTGATAAGAAGGCGGC	This paper	N/A
Mouse *Tln2* CRISPR sgRNA: AGGTGCGAACCAGAGCCTTG	This paper	N/A
Mouse *Tln2* CRISPR single-stranded donor: CACCCCACCCTGCCCATACCCCTCCTTACCACCAAGACGTGTT CTAGTAGGTCCAGGTAGCCCAAGGTGCATTCTGTGCCATA ATGCAAGGCTCTGGTTCGCACCTCTTCACTGACATCAGGGTA	This paper	N/A
Recombinant DNA		
DR274 vector	Addgene	#42250
pCXLE-hOCT3/4-shp53-F	Addgene	#27077
pCXLE-hSK	Addgene	#27078
pCXLE-hUL	Addgene	#27080
pCXLE-EGFP	Addgene	#27082
Software and algorithms		
Graph Pad Prism	GraphPad Software	GraphPad Prism, RRID:SCR_002798
ZiFiT targeter	Sander et al.[41]	http://zifit.partners.org/ZiFiT/
ImageJ	ImageJ	ImageJ, RRID: SCR_003070
LASX	Leica Application Suite X	Leica Application Suite X, RRID:SCR_013673
R (v3.6.0)	R Core	R Project for Statistical Computing, RRID: SCR_001905

(*Continued on next page*)

Continued

REAGENT or RESOURCE	SOURCE	IDENTIFIER
Vevo2100 ultrasound system	FUJIFILM VisualSonics Inc.	N/A
Episcopic confocal microscopy imaging systerm	Liu et al.[42]	N/A
Inference of CRISPR Edits (ICE)	Synthego	https://design.synthego.com
MERLIN Version 1.1.2	Abecasis et al.[43]	MERLIN, RRID:SCR_009289
BWA-MEM Version 0.7.15	Li and Durbin[44]	BWA, RRID:SCR_010910
GATK Version 3.4-0	Van der Auwera et al.[45]	GATK, RRID:SCR_001876
ANNOVAR	Wang et al.[46]	ANNOVAR, RRID:SCR_012821
BioRender	https://biorender.com	Biorender, RRID:SCR_018361
CNVnator	Abyzov et al.[47]	CNVnator, RRID:SCR_010821
Breakdancer	Chen et al.[48]	BREAKDANCER, RRID:SCR_001799
Seurat v3.2.1	Butler et al., 2018[49]	SEURAT, RRID: SCR_007322

RESOURCE AVAILABILITY

Lead contact

Further information and requests for resources and reagents should be directed to and will be fulfilled by the Lead Contact, Cecilia W. Lo (cel36@pitt.edu).

Materials availability

Additional materials are available from the lead contact upon request and without restriction.

Data and code availability

All raw sequencing data and genotype data generated in this paper have been deposited to the Sequence Read Archive (PRJNA624983) and are publicly available as of the date of publication. Publicly available single cell RNA sequencing data of human embryonic hearts were downloaded from https://www.spatialresearch.org/resources-published-datasets/doi-10-1016-j-cell-2019-11-025/, the single cell portal under accession number SCP1021 and NCBI database under BioProject: PRJNA576243, respectively. Accession numbers are listed in the Key resources table. This paper does not report original code. Any additional information required to reanalyze the data reported in this work paper is available from the Lead Contact upon request.

EXPERIMENTAL MODEL AND SUBJECT DETAILS

Human tissue

Blood for DNA extraction were obtained from patients at the University of Pittsburgh and University of Manchester with informed consent under human study protocols approved by the University of Pittsburgh and University of Manchester Institutional Review Board. The ASD family comprising 5 female and 6 male subjects were recruited from the Children's Hospital of Pittsburgh of UPMC with informed consent under a human study protocol approved by the University of Pittsburgh Institutional Review Board. An inhouse cohort of > 900 simple and complex CHD cases, including 94 inherited cardiomyopathy individuals (University of Pittsburgh) and 111 isolated ASD cases previously described (University of Manchester)[50] were screened for the *TPM1* mutation by either Sanger sequencing or via analysis of whole exome sequencing data if available.

Human cell lines

Human fibroblasts cells were generated from nasal scrape, which were obtained from one ASD proband (13-years-old female) and one healthy control (26-year-old male). iPSC lines were generated from fibroblasts cells.[51,52] All the iPSC cell lines have been cultured in mTeSR medium. Informed consent was obtained from both control and patient with human study protocol approved by the IRB of the University of Pittsburgh.

Xenopus embryo

Two-cell stage *X. laevis* embryos and *X. tropicalis* embryos at the 1 cell stage were obtained by *in vitro* fertilization from wild-type adult frogs from Chinese University of Hong Kong and Indiana University School of Medicine separately. Embryos of the same age were randomly assigned to experimental groups.

Mouse strain

Mouse zygotes for CRISPR gene editing were obtained from B6D2F1 mouse strain. Pseudopregnant female are of CD1 outbred strain background. All mice were housed and handled according to approved animal study protocols from the University of Pittsburgh and the Jackson Laboratory and in full compliance with Public Health Service policy on Human Care and Use of Laboratory Animals.

Animal study ethics approvals

All animal procedures were performed according to study protocols approved by the Institutional Care and Use Committee of the University of Pittsburgh, The Jackson Laboratory, Chinese University of Hong Kong and Indiana University School of Medicine.

METHOD DETAILS

Genome-wide linkage analysis

High density genotyping was performed using the Illumina Omni2.5-8 v1.3 BeadChip SNP Array. The genotype data generated comprising ~2.3 million SNP markers underwent quality control, filtering criteria and genotype error checking. We removed SNPs with MAF < 0.01, call genotyping rate < 99%, Hardy-Weinberg equilibrium p value < 0.00001, duplicated locus, and being on non-autosome and chromosome 6:28477796-33448353. In addition, SNPs with missing locus frequency in public database, existence of multiple alleles (> 2) and high linkage disequilibrium (LD) were eliminated. Using MERLIN,[43] parametric linkage analysis under autosomal dominant model with a penetrance of 1 and mutant allele frequency of 0.0001, and nonparametric linkage analysis were both implemented on a set of SNP genotypes. Focusing on candidate linkage regions, haplotypes were constructed using MERLIN.

Whole genome sequencing analysis, variant assessment, and variant confirmation

Library was constructed and sequenced to an average depth coverage of 43X per individual with 100-bp paired-end reads. Reads were aligned to the human reference genome (b37) using BWA-MEM algorithm.[53] GATK Best Practices including mark duplication and base quality score recalibration was performed to ensure accurate variant calling. SNP and InDel were detected by GATK Haplotypecaller.[45] Detection of copy number variants and structural variants were detected by CNVnator[47] and Breakdancer.[54] Variants were annotated using ANNOVAR.[46] Damaging segregating variants including nonsynonymous, stoploss, stopgain, splicing, frameshift, insertion/deletions were filtered for < 0.01 MAF in GnomAD.[55] The impact of variant was assessed using SIFT, PolyPhen-2, GERP++, and Combined Annotation Dependent Depletion (CADD).[56] Variant prioritization pipeline is listed in supplementary sheet. The K5del variant was confirmed using PCR amplification and Sanger dideoxy sequencing in the extended family members. Primers were listed in Key resources table.

Generation of antisense-morpholino gene knockdown in *Xenopus* embryos

Antisense-morpholino oligonucleotide (MOs) were designed and obtained from Gene Tools. Tpm1 translation blocking MOs (250 nM/cell) were injected into two-cell stage X. *laevis* embryos. The MO injected embryos and uninjected control embryos were observed on late stage 30's to early stage 40's under microscope for heart rate and edema. All embryos were harvested at mid stage 40's and fixed in 4% paraformaldehyde overnight for further histopathological analyses.

Generation of CRISPR-Cas9 gene-edited tpm1 *Xenopus* mutant embryos

Tpm1 sgRNA sequences were designed by the online tool ZiFiT targeter (http://zifit.partners.org/ZiFiT/). To assemble sgRNA, two oligonucleotides were annealed and linked to the linearized DR274 vector (Addgene #42250). After Dra1 digestion, the sgRNA-DR274 vector was used as template for *in vitro* transcription (MAXIscript T7 transcription kit, ThermoFisher). *Tpm1* sgRNA was purified and co-injected with Cas9 protein (PNA BIO Inc) into the X. *tropicalis* embryos at the 1 cell stage. To assess gene disruption efficiency, ten of the injected or uninjected embryos were harvested at stage 32 for western blot or T7E1 assay as previously described.[57] The CRISPR-Cas9 target region was also amplified from the extracted genomic DNA and analyzed by sequencing. The CRISPR-Cas9 injected embryos were observed on stage 42 under microscope for heart rate and edema. The Cas9 injected embryos were used as control. All embryos were harvested for further histopathological analyses in a similar fashion to the MO experiments. Assessment for ASD was carried out using ECM imaging as described below.

Generation of CRISPR-Cas9 gene-edited mouse embryos

For mouse CRISPR-Cas9 experiments, *Tpm1* and *Tln2* sgRNA DNA templates were designed by overlapping PCR with a forward primer containing a T7 promotor and the guide sequence and a common reverse primer with the stem loop. B6D2F1 oocytes were collected in KSOM medium (Millipore, Cat # MR-121-D) and electroporation was conducted in Opti-MEM medium containing Cas9 protein 100 ng/μl (Alt.R S.p. Cas9 Nuclease 3NLS IDT Cat # 1074181), Tpm1 sgRNA 200 ng/μl, Tpm1 ssODN 200 ng/μl, Tln2 sgRNA 200 ng/μl, Tln2 ssODN 200 ng/μl. The electroporation was performed using the Super electroporator NEPA21 type II and CUY 501-1-1.5 electrode (NEPA GENE Co. Ltd, Chiba, Japan) using the following settings: poring pulse (voltage 40 V, pulse length 2.5 ms, pulse interval 50 ms, number of pulses 4, decay rate 10%, polarity +); transfer pulse (voltage 7V, pulse length 50 ms, pulse interval 50 ms, number of pulses 5, decay rate 40%, polarity +/ =). After electroporation, the embryos were washed two times in KSOM

medium, then cultured in KSOM medium overnight at 5% CO2 and 37°C. In the following day, the two cell stage embryos were transferred to the oviducts of pseudopregnant CD1 females (0.5 dpc). The pseudopregnant mothers were then examined by ultrasound imaging to track development and viability of the embryos start at E6.5-7.5 onward. All Cas 9 guide RNA and single stranded donor sequences are provided in Key resources table.

Phenotyping and genotyping CRISPR-Cas9 mouse embryos

Noninvasive in utero fetal ultrasound imaging with the Vevo2100 ultrasound system using previously described method[58] was used to track development and viability of CRISPR-Cas9 targeted mouse embryos. Ultrasound scanning was initiated at day E7.5/8.5, with daily scans performed to track development and viability of the embryos. The number of conceptuses on initial scan is counted and tracked on successive days to determine long term viability. Heart beating is initiated on E8.5 and can easily detected by ultrasound imaging. Embryos without heart beat at E8.5, usually die and are resorbed between E9.5-10.5, with finding of severe pericardial effusion and hydrops indicating heart failure and imminent death. Litters were harvested at different stages for phenotype/genotype analyses. Embryos were fixed in 4% paraformaldehyde, with the E8.5-9.5 embryos processed for whole mount immunostaining. Embryos collected at later gestation were paraffin embedded for imaging by episcopic confocal microscopy for 2D and 3D histological reconstructions.[42]

Episcopic confocal microscopy histological analysis

Paraformaldehyde fixed embryos were embedded in paraffin and then sectioned and imaged using episcopic confocal microscopy (ECM) as previously described.[59] ECM imaging provided serial 2D histological image stacks that were then digitally resectioned in different imaging planes and 3D reconstructed in different view for assessing cardiovascular anatomy and diagnosis of structural heart defects. This served as the gold standard for CHD diagnosis. For mouse embryos, paraffin sections were also collected during ECM imaging for additional immunohistology and DNA extraction for assessing CRISPR gene editing efficiency.

Assessment of CRISPR gene editing efficiency in mouse embryos

For assessing the efficiency of CRISPR mediated KI/KO in E8.5-9.5 embryos, tissue was microdissected from the caudal region of the embryo 5-7 sections spanning the heart, including the atria, were processed for DNA extraction (QIAGEN, #56404, QIAamp DNA FFPE tissue kit), followed by PCR DNA amplification using mouse *Tpm1* and *Tln2* genotyping primers (Key resources table). The DNA products generated were further analyzed by Sanger sequencing and the sequence trace files were analyzed using Inference of CRISPR Edits (ICE), an online CRISPR gene editing analysis tool from Synthego (https://design.synthego.com).[59] This provided computational analysis of the recombination events, allowing determination of the KI and KO frequencies.

Immunostaining

For whole mount fluorescent immunostaining, embryos were fixed overnight in 4% paraformaldehyde at 4°C and processed as described previously.[26] Entire embryos and/or paraffin-embedded tissues were incubated with primary antibodies to TPM1 (Abcam, #ab55915, 1:500), α-actinin (Sigma-Aldrich, #A7811, 1:500), and pH3 (Millipore, Ser10, #2664259, 1:100). Secondary antibodies used were AF555 goat anti-rabbit IgG (A-21428, 1:1000) and AF647 goat anti-mouse IgG1 (A-21240, 1:1000). DAPI was used to visualize nuclei. Whole mount embryos and sections were imaged with confocal microscopy and quantitatively analyzed with ImageJ.[60]

Human iPSC and iPSC-CM production

Human fibroblasts or lymphoblastoid cells were transfected with four episomal plasmids (Addgene: #27077 (pCXLE-hOCT3/4-shp53-F), 27078 (pCXLE-hSK), 27080 (pCXLE-Hul), 27082 (pCXLE-EGFP)) using electroporation.[61] After 7 days these cells are switched to a 6-well plate with mTESR1 media and transferred to hypoxic conditions. After 21-40 days, iPSC clone was formed and alkaline phosphatase staining positive colonies were picked up at day 40. The clone was chosen and expanded in 24-well plates coated with feeder cells or BD Matrigel with mTESR1 media. Pluripotency of iPSCs was identified by immunofluorescent staining and quantitative PCR analysis.[62] The continuous culture of iPSC cells (15-45 passages) underwent monolayer cardiomyocyte differentiation method.[63] Clusters of beating cardiac myocytes were observed after 8 days of differentiation. All the assays were then tested on the following days (day 18-22).

Analysis of human iPSC-CM

Cell proliferation was assessed by immunofluorescence staining of paraffin-embedded sections with antibodies to pH3 (1:100) and Ki67 (Abcam, #ab15580, 1:500). Secondary antibodies included goat anti-rabbit IgG (Invitrogen, #A21429, 1:1,000) and goat anti-mouse IgM (Invitrogen, #A21042, 1:1,000). DAPI staining was used for visualization of cell nuclei and cells in anaphase or telophase versus prometaphase or metaphase. Apoptosis was analyzed with terminal deoxynucleotidyl transferase-mediated dUTP-biotin nick-end labeling (TUNEL) with a TUNEL assay kit (Roche, #12156792910). Sections were imaged with confocal microscopy and quantitatively analyzed with ImageJ.[60] All primer sequences are provided in Table S5.

Transcript and protein analysis

Total RNA was isolated from iPSC-CM using Trizol reagent according to the manufacturer's instructions (Invitrogen, Carlsbad, CA, USA), and subjected to real-time quantitative reverse transcription PCR according to the standard protocols. Each sample was performed in triplicate. Relative expression of RNA was normalized to GAPDH level. Primers used are listed above. Protein was extracted and separated on 10% SDS-PAGE gels, and western blot was performed as previously described. Primary antibody against TPM1 was used to detect the protein. Densitometry analysis was performed with ImageJ.[60]

Single-cell RNA-sequencing data analysis

Publicly available single-cell RNA sequencing (scRNA-seq) datasets of human embryonic hearts at 6.5, 12 and 19-21 postconceptional weeks (PCW) were analyzed for cardiomyocyte co-expression of *TPM1* and candidate protective genes.[30–32] Cell type annotation and gene-UMI count sparse matrix files of scRNA-seq datasets at 6.5 and 12 PCW were directly downloaded[30] or obtained from the single cell portal under accession number SCP1021,[31] respectively. Raw sequencing data from scRNA-seq dataset at 19-21 PCW were downloaded from NCBI database under BioProject: PRJNA576243 and re-processed as described in the original paper[32] to generate cell type annotation and count matrix files, as these two files were not available. Downstream analyses were performed on all three independent scRNA-seq datasets. The sum of UMI counts for each cell was normalized to 10,000 and then log-transformed. Differentially expressed genes (DEGs) in human cardiomyocytes against all other cell types were identified with the Wilcoxon Rank Sum test using Seurat "FindAllMarkers" function[49] with default parameters. An adjusted $p < 0.0001$ was considered statistically significant.

QUANTIFICATION AND STATISTICAL ANALYSIS

The animal experiments were not randomized, but the investigators were blinded to sample allocation. D'Agostino & Pearson normality test and Shapiro-Wilk normality test were used to test if the data had a Gaussian distribution. For Gaussian distribution, comparison was conducted with unpaired Student's t test. For Non- Gaussian distribution, comparisons were conducted with non-parametric Mann-Whitney test (two-tailed). *P* values for t tests are reported in the respective figures, and $p < 0.05$ were considered statistically significant.